Sacrificial mold-assisted 3D printing of stable biocompatible gelatin scaffolds

Sakthivel Nagarajan, Habib Belaid, Socrates Radhakrishnan, Catherine Teyssier, Sebastien Balme, Philippe Miele, David Cornu, Narayana Kalkura Subbaraya, Vincent Cavaillès, Mikhael Bechelany

Sacrificial Mold-Assisted 3D Printing of Stable Biocompatible Gelatin Scaffolds

Sakthivel Nagarajan [1], Habib Belaid [1,3], Socrates Radhakrishnan [2], Catherine Teyssier [3], Sébastien Balme [1], Philippe Miele [1], David Cornu [1], Narayana Kalkura Subbaraya [2], Vincent Cavaillès [3] and Mikhael Bechelany [1,*]

[1] Institut Européen des Membranes, IEM, UMR 5635, Univ Montpellier, CNRS, ENSCM, Place Eugene Bataillon, F-34095 Montpellier cedex 5, France ; nagarajan.sakthivel@outlook.com (N.S), habib.belaid@umontpellier.fr (H.B), sebastien.balme@umontpellier.fr (S.B), philippe.miele@umontpellier.fr (P.M), david.cornu@enscm.fr (D.C)

[2] Crystal Growth Centre, Anna University, Chennai, India, 600025; biot.socrates@gmail;com (S.R), kalkurasn@annauniv.edu (S.N.K)

[3] IRCM, Institut de Recherche en Cancérologie de Montpellier, INSERM U1194, Université Montpellier, Montpellier F-34298, France ; catherine.teyssier@inserm.fr (C.T), vincent.cavailles@inserm.fr (V.C)

* Correspondence: mikhael.bechelany@umontpellier.fr, Tel: +33-46-714-9167; Fax: +334-67-149-119

Abstract: Gelatin is a fascinating biomaterial due to its biocompatibility, biodegradability and chemical composition. The engineering of gelatin scaffolds with the most appropriate architecture is crucial for tissue engineering applications. Currently available porogen assisted scaffold fabrication technique are limited for the fabrication of repeatable and customized scaffolds. Three dimensional printing is an appropriate technique to prepare customized structure. In this report, customized gelatin scaffolds were fabricated using 3D printed polyvinyl alcohol (PVA) sacrificial molds. Gelatin was stabilized through crosslinking and the PVA was solubilized to obtain 3D customized gelatin scaffolds. The gelatin scaffolds displayed tunable pore size from 350 to 1200 μm. The influence of PVA infill density on the gelatin scaffold porous structure and interconnectivity was also analyzed. Furthermore, the gelatin scaffold stability in phosphate buffered saline solution and their swelling capacity demonstrated that they were effectively crosslinked. The scaffold cytocompatibility and the good cell attachment and proliferation on these scaffolds showed that the sacrificial mold-assisted 3D printing is suitable for producing customizable gelatin scaffolds for biomedical applications.

Graphical Abstract

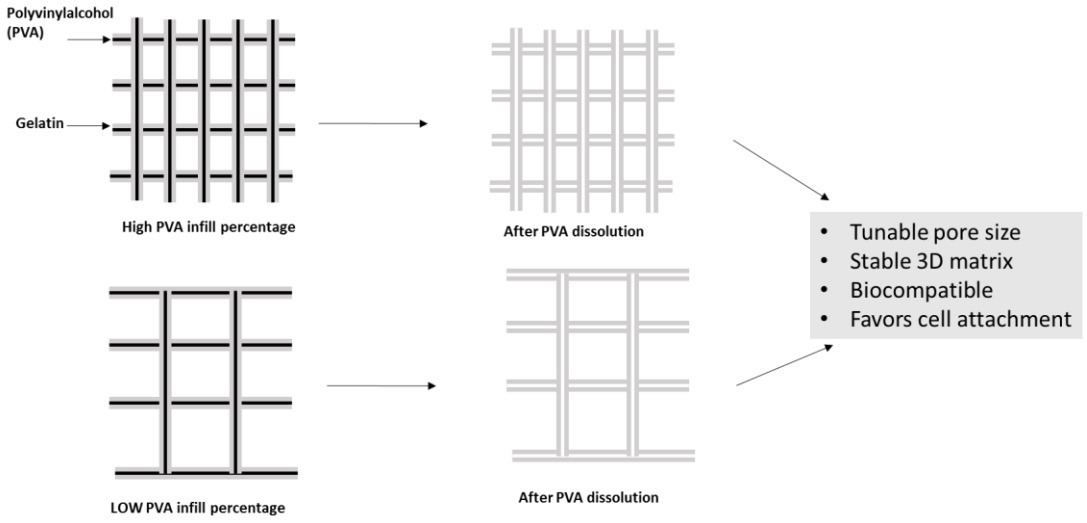

Keywords: 3D printing; fused deposition modeling; gelatin; sacrificial mold; polyvinyl alcohol

1. Introduction

The major shortcoming of two-dimensional (2D) cell culture models is their inability to emulate the 3D cell environment of tissues [1, 2]. Conversely, 3D cell culture approaches almost recapitulates the complex mechanical and chemical environment of tissues, and this is crucial for drug screening and tissue engineering [3]. Polymer-based scaffolds also mimic the 3D cell culture environment. For instance, scaffolds fabricated with synthetic or bio-based polymers are often used as templates for tissue regeneration. However, 3D engineering methods can be advantageously employed to fabricate scaffolds that allow cell infiltration and nutrient transport.

Scaffolds have been fabricated using various techniques, such as particulate leaching, freeze-drying, phase separation, gas foaming and electrospinning [4], that permit the formation of interconnected porous structures and tunable pore size. However, it is difficult to fabricate reproducible structures and to control the interconnected porosity [4]. This issue could be solved by selecting 3D printing technologies [5, 6], representing advantageous tools for the production of reproducible and controlled structures. 3D printed sacrificial molds or sacrificial mold-assisted techniques have been widely used for manufacturing microfluidic channels, polymeric scaffolds, inorganic 3D matrix materials, and microneedles [7-10].

Gelatin and collagen are highly attractive biopolymers for scaffold production because they are inherently biocompatible and biodegradable. They also contain the Arg-Gly-Asp (RGD) motif and matrix metallo protease degradable molecule that can facilitate the cell-scaffold interaction. 3D printing of gelatin using the fused deposition modeling (FDM) technique is arduous due to the lack of sharp melting temperature of gelatin. Gelatin has been employed for ink-based 3D printing [11], which requires surface modification of gelatin [12]. Unmodified gelatin is printable below ambient temperature but additional crosslinking after the printing is mandatory to stabilize the 3D scaffolds. However, the porous structure is obtained only through the inter filament gap in extrusion 3D printing. Interestingly, dissolution of the sacrificial mold results in interconnected porous gelatin scaffolds by connecting multiple layers through hollow tubes.

On the other hand, gelatin scaffolds could be easily fabricated using polyvinyl alcohol (PVA) sacrificial molds printed using the FDM technique. PVA is a water-soluble thermoplastic suitable for the 3D printing of complex structures with high degree of control using the thermal extrusion method [8]. It has been widely used to produce sacrificial molds for the fabrication of poly(dimethyl siloxane) scaffolds [7, 8, 13], but not of 3D biopolymer scaffolds. Li et al. attempted to embed 3D-printed PVA filaments in a gelatin matrix to obtain perfusable vascular-like structures upon PVA dissolution [14]. However, fabrication of self-standing interconnected porous gelatin scaffolds with controlled architecture has not been reported previously. In a recent work, Jung et al. described photocurable and alkaline soluble sacrificial molds for the fabrication of gelatin/polycaprolactone 3D scaffolds.

They used sodium hydroxide for the dissolution of the sacrificial mold, and they often observed permanent deformation of the scaffolds. Moreover, the fabrication of gelatin scaffolds was difficult [15]. Therefore, developing an appropriate method to fabricate customized gelatin scaffolds is crucial.

Besides PVA, various other materials are employed for sacrificial mold fabrication. For example, perfusable complex vascular architectures were 3D printed using water-soluble sugar glass as sacrificial mold and gelled polydimethylsiloxane. Dissolution of the sacrificial mold led to a self-standing structure that could be perfused [16]. Similarly, monolithic microfluidic channels were fabricated using 3D printed water-soluble sugar-based sacrificial molds [17]. However, these studies did not investigate the fabrication of biopolymer-based interconnected porous scaffolds. Thermo-responsive polymers also have been used as sacrificial molds. For instance, poloxamer 407 (Pluronic F127) displays characteristic properties of gel to sol transformation upon cooling that favor the easy removal of the sacrificial mold [18].

In this report, a sacrificial mold-assisted 3D printing method was used to fabricate self-standing water-insoluble gelatin scaffolds with tunable pore size and porosity. The PVA-based sacrificial molds were 3D printed using the FDM technique and different polymer infill densities. The influence of PVA infill density on the gelatin scaffold pore size was evaluated, followed by analysis of the gelatin scaffold swelling capacity in phosphate buffered saline (PBS). In addition, the gelatin scaffold biocompatibility and cell attachment were studied using cell staining and scanning electron microscopy (SEM).

2. Materials and Methods

Gelatin (9000-70-8), glutaraldehyde (25%, 111-30-8), absolute ethanol, glacial acetic acid (100%, 64-19-7), hexamethyldisilazane (≥99%, 999-97-3), PBS, DMSO and calcein-AM solution were purchased from Merck and used as received. The cell culture reagents were MEM alpha medium, penicillin/streptomycin and trypsin-EDTA (all from Gibco) and fetal bovine serum (Eurobio). PVA filament was from Makershop.

2.1. 3D printing of sacrificial PVA molds

Sacrificial PVA molds were fabricated using PVA filament and a Prusa Research MK2S 3D printer (see Table 1 for the 3D printing parameters). Computer-aided design software (Design Spark Mechanical) was used for drawing the PVA molds and the STL file was generated using the Prusa3Dslicer software. The final dimensions of the PVA sacrificial mold are 10 mm length, 10 mm depth and 6 mm height. Each batch of PVA molds requires 8 minutes to be printed.

Table 1. 3D printing parameters.

Parameters	Value
First layer height	0.1 mm
Other layers' height	0.2 mm
Perimeters	1
Number of top & bottom layers	0 & 5
Infill percentage	40% and 55%
Combine infill layers	3
Infill angle	45°
Bed temperature	60 °C
Nozzle temperature (1st layer)	215 °C
Nozzle temperature (other layers)	210 °C

2.2. Fabrication of 3D gelatin scaffolds

The gelatin solution (10% w/v) was prepared at 60 °C using glacial acetic acid as solvent. The 3D PVA molds fabricated with 40% and 55% of PVA infill density were denoted as PVA40 and PVA55, respectively. Then, the gelatin solution (100µL/PVA mold) was poured and let to fill the PVA molds. PVA molds filled with the gelatin solution were dried at room temperature for 24 hours, and then crosslinked using 0.5% glutaraldehyde solution (3 mL/4 molds) for 24 hours. The glutaraldehyde solution was prepared from 25% (v/v) glutaraldehyde stock solution using absolute ethanol. Finally, the crosslinked gelatin-filled PVA molds were immersed in water at 50°C, and this step was repeated five times to completely dissolve the mold. PVA dissolution resulted in water-insoluble gelatin scaffolds. Gelatin scaffolds fabricated using PVA40 and PVA55 sacrificial molds were denoted as G40 and G55, respectively (Figure 1).

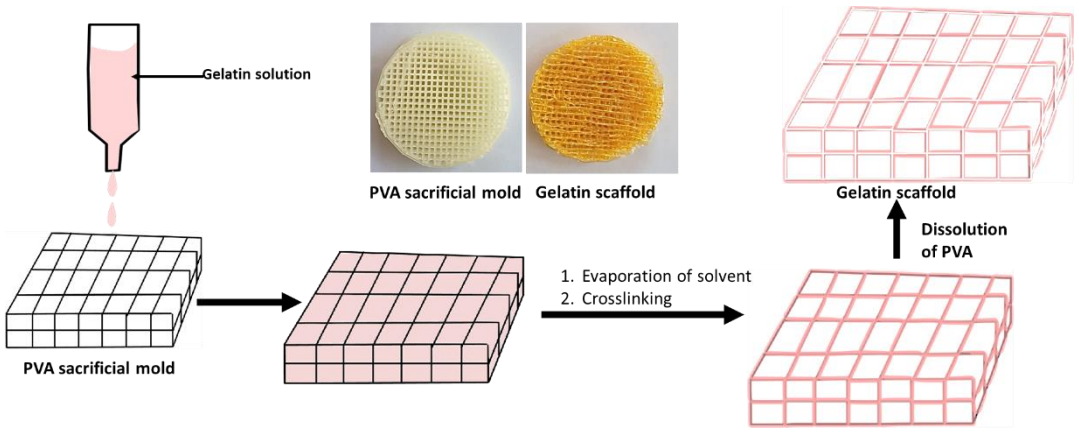

Figure 1. Schematic representation of gelatin scaffold fabrication.

2.3. Gelatin scaffold characterization

The morphology of the PVA sacrificial molds and gelatin scaffolds were analyzed by SEM (HITACHI S4800) after coating with platinum using an ion sputter coater. The 3D architecture of the scaffolds was analyzed using EasyTom XL 150.The gelatin scaffold swelling ratio was calculated by equilibrating pre-weighed gelatin scaffolds in 0.1 M PBS at pH 7.4 at 37 °C. At different time points, equilibrated samples were removed and the weight of the scaffolds was recorded. The scaffolds were carefully put back in PBS after weight recording.

The swelling ratio was calculated with the following equation (1):

$$\text{Swelling Ratio} = \frac{Wt - W0}{W0} \times 100 \quad (1)$$

where Wt is the gelatin scaffold weight at the 't' time, and Wo is the gelatin scaffold initial weight.

Fourier-transform infrared spectroscopy (FTIR) spectra of gelatin scaffolds were recorded at 600 to 4000 cm^{-1} frequency and 4 cm^{-1} resolution using a NEXUS instrument, equipped with an attenuated total reflection accessory.

2.4. Cell viability assays

MG63 osteosarcoma cell line (obtained from ATCC) were cultured in MEM alpha medium supplemented with 1% penicillin/streptomycin (Gibco 15140-122) and 10% fetal bovine serum (Eurobio CVFSVF00-01) at 37 °C in 5% CO_2. Cells were maintained in 10 cm diameter dishes and 0.05% trypsin-EDTA (Gibco 25300-054) was used for passaging. Gelatin scaffolds were sterilized with 60% ethanol (w/v) and rinsed in PBS. For cell viability assays, $1.5x10^3$ MG63 cells/well were plated in 96-well plates and let to attach for 24 hours. Then, the sterilized gelatin scaffold was put on top of the cell layer and cell viability was assessed with the MTT ((3-(4,5-dimethylthiazol-2-yl)-2,5-diphenyl tetrazolium bromide) assay at 1, 4 and 8 days (n=3). Briefly, cells were incubated with 0.05 mg mL^{-1} of MTT solution (100 µL/well) for 2h to allow the formation of purple-colored formazan crystals. Then, formazan crystals were dissolved by adding 100 µL/well of dimethyl sulfoxide (BDH Prolab 23486.297), and absorbance was recorded at 560 nm using a Multiskan plate reader (Thermo Scientific, USA).

2.5. Calcein staining to monitor cell attachment and proliferation

MG63 cells ($5x10^3$ cells/scaffold) were cultured on gelatin scaffolds for 4 days. Then, they were incubated with the calcein-AM solution (maker) at 37 °C in 5% CO_2 for 30 minutes and monitored by epifluorescence microscopy (DM6000 Leica). SEM was also used to characterize the cells attached on the scaffolds. Briefly, cells cultured on scaffolds were fixed with 2% glutaraldehyde solution for 1 hour and then scaffolds were washed with PBS. Cells attached to the scaffolds were incubated with

increasing ethanol concentrations (10%, 20%, 40%, 70% and 90% (v/v)), followed by drying using hexamethyldisilazane.

3. Results and Discussion

Gelatin scaffolds were 3D printed using PVA sacrificial molds with a porous structure that were then dissolved in water. Designing scaffolds with appropriate pore size and properties allowing cell adhesion and proliferation is essential for their use in tissue engineering. For instance, Murphy et al. reported that high pore size (> 300 μm) facilitates cell infiltration and proliferation, vascularization and bone ingrowth [19]. Therefore, to obtain tunable pore size, two different PVA molds with different polymer infill density (40% and 55%) were used (PVA40 and PVA55, respectively). The morphology of the PVA molds (Figure 2a and d) and gelatin scaffolds (Figure 2b and e) was analyzed by SEM. The gelatin scaffolds displayed a tunable pore size ranging from 350 to 1200 μm (Figure 2c and f) which shows that the gelatin scaffolds are suitable to facilitate cell infiltration. Although gelatin is highly water soluble, the crosslinked gelatin scaffolds maintained the architecture and porous morphology even after dissolution of the PVA sacrificial molds, highlighting their stability in aqueous solution. Sacrificial PVA molds generate the porous structure to the gelatin scaffolds in three ways: I. dissolution of sacrificial mold filament leads to the hollow filament of gelatin, II. Inter gelatin filament gap and III. Dissolution of sacrificial filament junction supports to connect adjacent layers of gelatin filaments. Such interconnectivities are crucial for cell migration and infiltration into multiple layers of scaffolds.

The architecture of the gelatin scaffolds was the replica of the PVA sacrificial molds and the number of pores per unit area in each scaffold (G40 and G55) correlated with their number in the corresponding sacrificial mold (PVA40 and PVA55). However, the pore number in any given area was higher in the gelatin scaffolds than in the PVA sacrificial molds, due to the shrinkage of the gelatin scaffold during drying (Figure 2a to f).

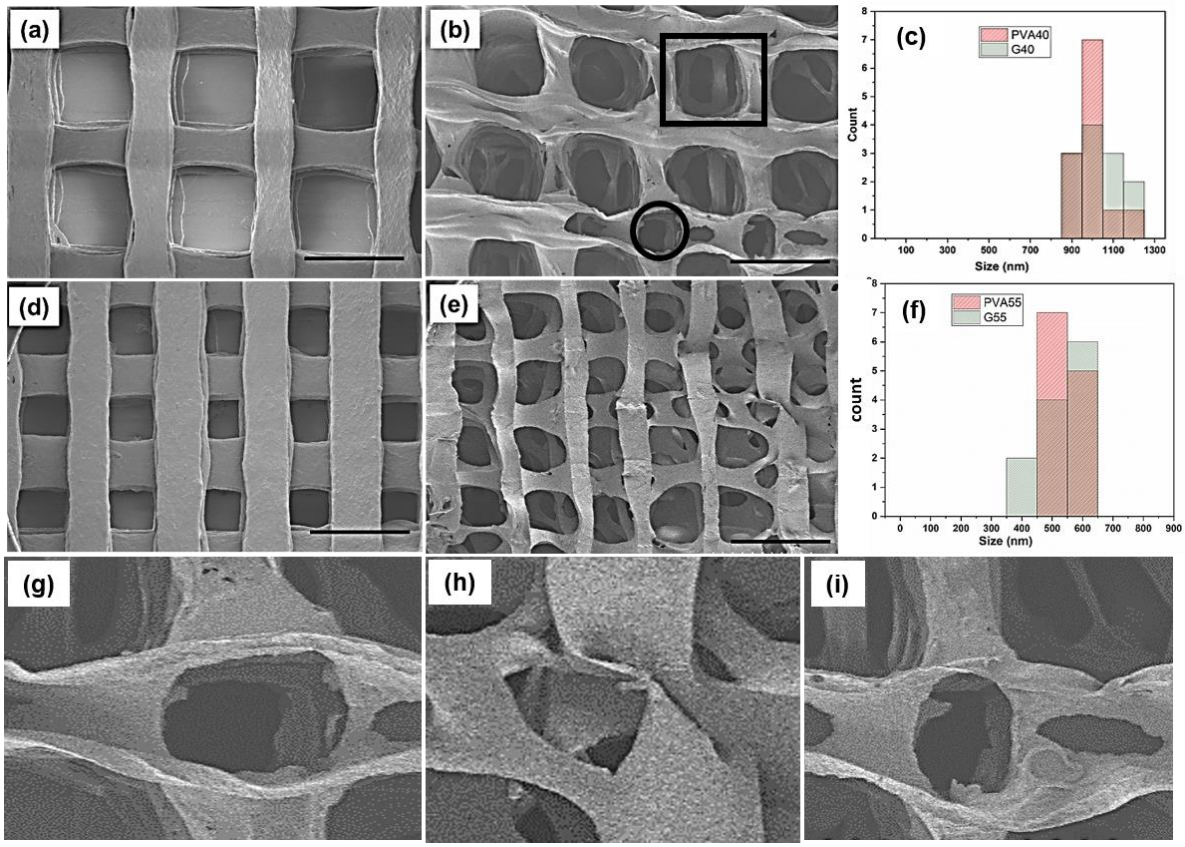

Figure 2. SEM images of PVA40 (a), G40 (b,g,i), PVA55 (d), G55 (e,h), and pore size distribution in sacrificial PVA molds and gelatin scaffolds (c and f).

Analysis of the 3D architecture of the G40 and G55 scaffolds by X-ray microtomography (Figure 3) showed that both gelatin scaffold types had a porous structure imparted by the porous structure of the PVA sacrificial molds (see PVA40 and PVA55 images in Figure 2a and 2d). This type of pore is indicated by black squares in Figures 2 and 3a. Moreover, a second pore type was formed after PVA dissolution (black circles in Figure 2 and 3a). Indeed, the gelatin deposited and crosslinked around the PVA matrix during scaffold synthesis formed gelatin tubes after PVA dissolution (Figures 2g to i). The microtomography images of G40 and G55 scaffolds showed that gelatin uniformly diffused in the two types of sacrificial molds (Figure 3). It shows that preparation of gelatin solution in glacial acetic acid prevented the dissolution of sacrificial mold before crosslinking of gelatin. Further, high solubility of PVA in water favors the gelatin scaffolds formation. As observed also on the SEM images, the gelatin scaffold pores were strongly influenced by the PVA sacrificial mold porosity (compare Figure 3a and c). The two pore types (inter- and intra-gelatin tubes, indicated by the square and circle, respectively, in Figure 3) were clearly larger in G40 than in G55 scaffolds.

Moreover, the two scaffolds presented a 3D interconnected porous structure (Figure 3b and d). The tubes formed after dissolution of the PVA sacrificial molds were observed along the rows and columns and introduced a high interconnectivity within the scaffolds. The PVA sacrificial mold

were 3D printed in such a way that the two adjacent layers were separated by a specific distance. This helped to interconnect the porous structures formed between gelatin tubes. Presence of these interconnected porous structures is crucial to facilitate cell infiltration.

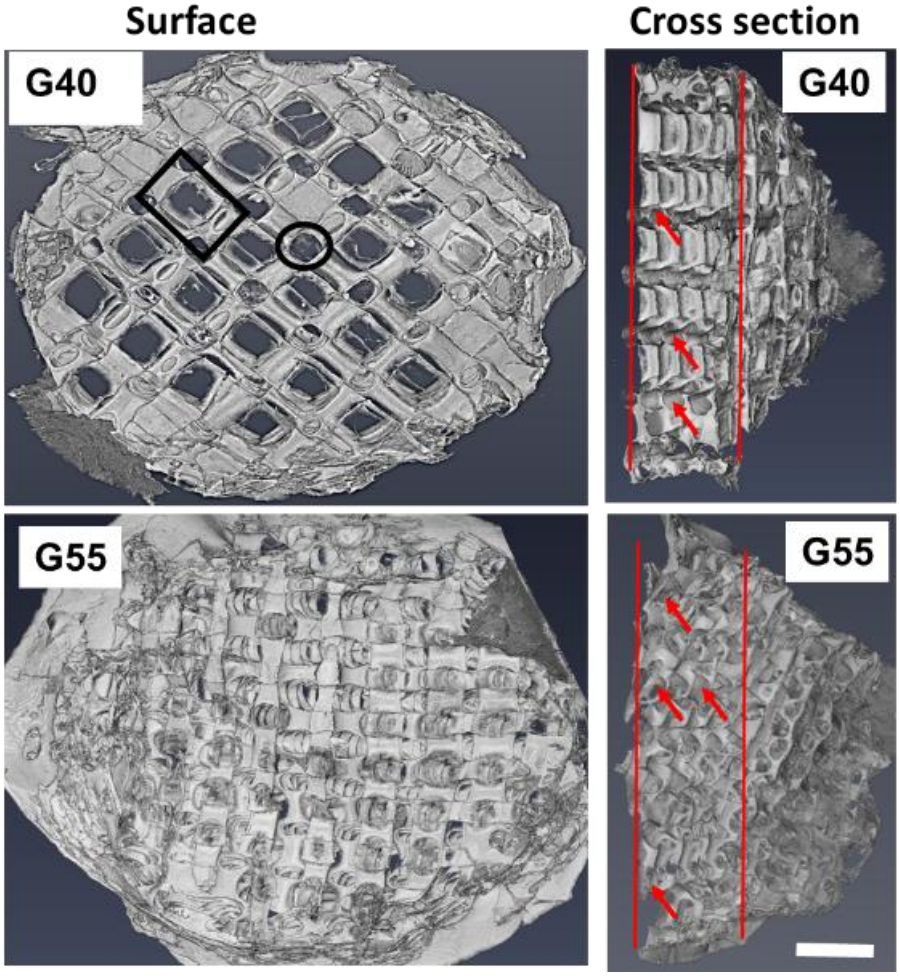

Figure 3. X-ray microtomography images of gelatin scaffolds (scale bar is 2 mm). The cross-sectional area is delineated by the red lines; arrows indicates the porous structure.

FTIR spectra of the G40 and G55 gelatin scaffolds (Figure 4a) showed, as expected [20], the presence of peaks characteristic of gelatin (amide I and amide II at 1650 cm^{-1} and 1539 cm^{-1}, respectively). C-H stretching vibration of the alkyl group of PVA was also observed at 2921 cm^{-1} and 2851 cm^{-1} [21]. Although SEM images (Figure 2) clearly confirmed PVA dissolution and the formation of gelatin tubes, FTIR indicated that some PVA molecules were still attached to the gelatin scaffolds. The primary amine groups in gelatin are responsible for the crosslinking. Conversely, the hydroxyl groups of PVA react less with glutaraldehyde compared with the gelatin amine groups. Many studies reported that PVA crosslinking is an acid-catalyzed reaction and that it requires high glutaraldehyde concentrations [22, 23]. Here, crosslinking was performed with a high concentration of glutaraldehyde (0.5% solution), which might explain the fact that traces of PVA are covalently

attached to gelatin. Decreasing the glutaraldehyde concentration could diminish the PVA attachment on the gelatin scaffolds.

Analysis of the gelatin scaffold swelling capacity showed that G40 scaffolds reached the swelling equilibrium after 1 day in PBS (Figure 4b). By contrast, the G55 scaffold exhibited a significantly lower swelling ratio (approximately 2-fold less as compared to the G40 scaffold) after 1 day in PBS (Figure 4b). Interestingly, the swelling capacity of the G55 scaffold increased upon time (increase of the swelling ratio up to 12 days in PBS). This delay in the swelling capacity of the G55 scaffold can be explained due to the increased degree of crosslinking compare to G40. Of note, both the G40 and G55 scaffolds did not exhibit significant weight loss even after 12 days in PBS and remained easily manipulable (Figure 4b), thus indicating that they are insoluble and validating their stability in solution.

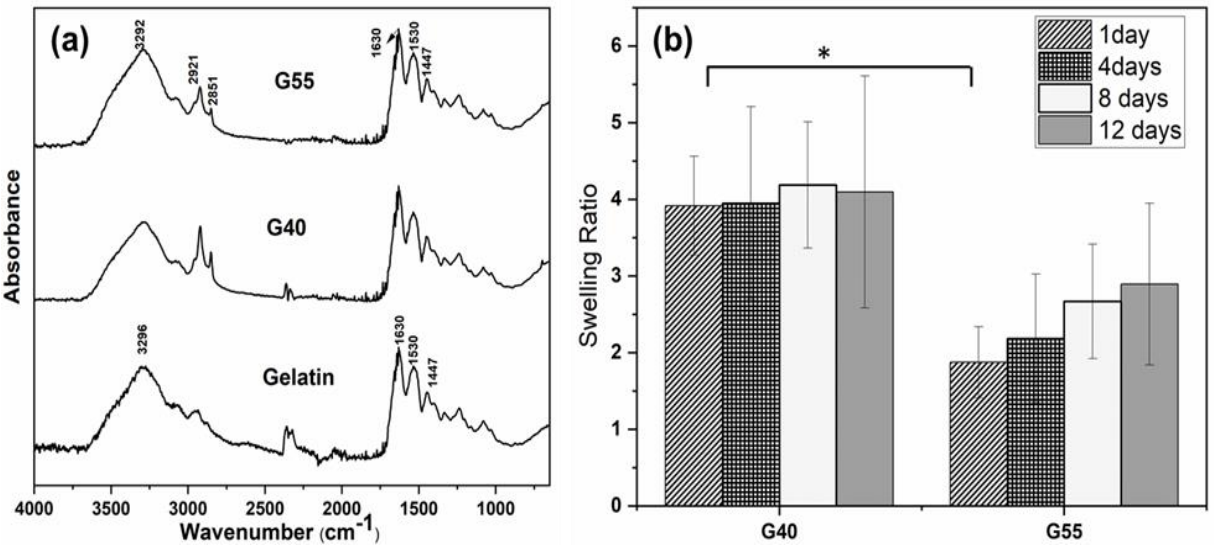

Figure 4. FTIR spectra (a) and swelling analysis (b) of the indicated 3D gelatin scaffolds (*p<0.05).

As glutaraldehyde crosslinking might alter the cytocompatibility of gelatin scaffolds, the effect of the scaffold on MG63 cell viability was analyzed with the MTT assay (Figure 5a). The viability of MG63 cells grown in the presence of the G40 scaffold for up to 8 days was comparable to that of cells cultured in the absence of scaffold (control). This proved that glutaraldehyde crosslinking did not affect significantly cell viability.

Moreover, epifluorescence microscopy and SEM analysis after calcein staining showed that MG63 cells could attach and proliferate on the G40 scaffold (Figure 5b and c). These findings confirm the cytocompatibility of the G40 scaffold. In general, scaffolds are functionalized with cell adhesion molecules to facilitate cell attachment. As gelatin contains the RGD (Arg-Gly-Asp) binding motif for

integrin [24, 25], no additional functionalization of these gelatin scaffolds is required for cell attachment.

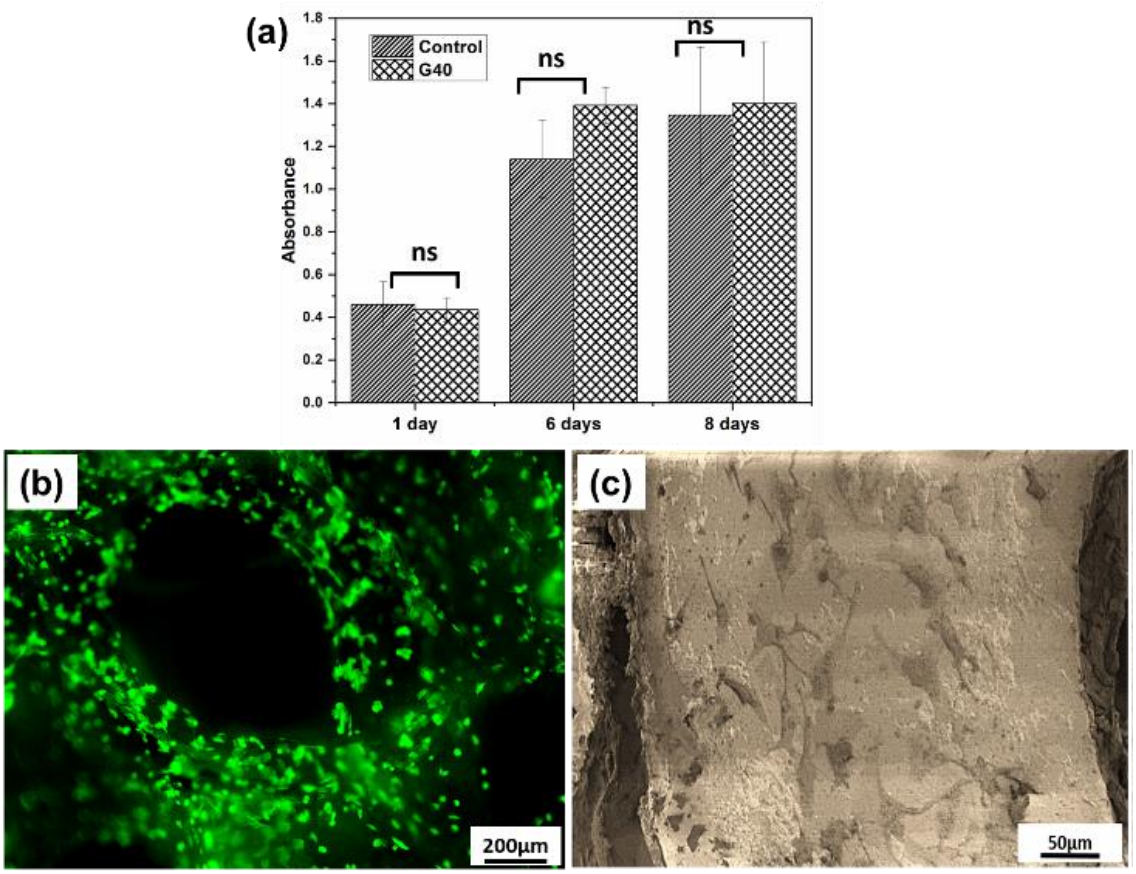

Figure 5. Cell viability and attachment on 3D gelatin scaffolds (G40) analyzed with the MTT assay (a), and by calcein staining: epifluorescence microscopy image (b) and SEM image showing cells attached on the G40 scaffold (c), ns=no significance (statistical analysis was performed using student t test).

4. Conclusions

The engineering of the scaffolds with an interconnected pore network and appropriate pore size is essential to facilitate cell infiltration, and the transport of nutrients and wastes. Many studies reported that scaffolds with a pore size higher than ~300 µm are optimal for bone tissue engineering because they significantly reduce cell aggregation and facilitate cell proliferation and vascularization [19, 26-29].

The work presented here shows that the cautious engineering of sacrificial molds allows the fabrication of gelatin scaffolds with tunable pore size and architecture suitable for tissue engineering applications. The synthesized gelatin scaffolds displayed interconnected pores with a pore size between 400 and 1200 µm, and were stable in PBS as assessed by swelling assay. Assays using MG63 osteoblastic cells showed that such scaffolds are biocompatible, and allow cell attachment and proliferation without addition of any cell adhesion molecule. In conclusion, this study provides a method to develop engineered stable interconnected porous gelatin scaffolds using sacrificial mold-

assisted 3D printing. Further, this approach could be extended for the fabrication of customized scaffolds using various other biopolymers or synthetic polymers. Human organs display multiple biopolymeric composition as well as gradient composition in their scaffold matrix [30]. Synthesis of such complex scaffolds could be attempted using sacrificial mold technique. Electrical simulation found to improve the nerve tissue regeneration and conducting polymer-based particles are highly biocompatible [31-34]. Such particles could be mixed with biopolymers for the conductive scaffolds fabrication using sacrificial mold assisted technique. These scaffolds could be loaded with therapeutic molecules and employed for wound healing and skin tissue engineering applications.

Acknowledgment: The authors acknowledge the financial support by the Indo-French Centre for the promotion of advanced research-Cefipra (Project 5608-1). One of the authors (NKS) thank the University Grants Commission, India for the award of UGC-BSR Faculty Fellowship. The University of Montpellier (MUSE "3DTraitCancer") also supported this study. We acknowledge the members of the MRI facility of the national infrastructure France-BioImaging supported by the French National Research Agency (ANR-10-INBS-04, «Investments for the future»), the Labex CEMEB (ANR-10-LABX-0004) and NUMEV (ANR-10-LABX-0020).

Conflicts of Interest: The authors declare no conflict of interest.

References

1. Edmondson, R.; Broglie, J.J.; Adcock, A.F.; Yang, L. Three-Dimensional Cell Culture Systems and Their Applications in Drug Discovery and Cell-Based Biosensors. ASSAY and Drug Development Technologies 2014, 12, 207-218, doi:10.1089/adt.2014.573.
2. Mirbagheri, M.; Adibnia, V.; Hughes, B.R.; Waldman, S.D.; Banquy, X.; Hwang, D.K. Advanced cell culture platforms: a growing quest for emulating natural tissues. Materials Horizons 2019, 6, 45-71, doi:10.1039/C8MH00803E.
3. Fang, Y.; Eglen, R.M. Three-Dimensional Cell Cultures in Drug Discovery and Development. SLAS DISCOVERY: Advancing Life Sciences R&D 2017, 22, 456-472, doi:10.1177/1087057117696795.
4. Deb, P.; Deoghare, A.B.; Borah, A.; Barua, E.; Das Lala, S. Scaffold Development Using Biomaterials: A Review. Materials Today: Proceedings 2018, 5, 12909-12919, doi:https://doi.org/10.1016/j.matpr.2018.02.276.
5. Belaid, H.; Nagarajan, S.; Teyssier, C.; Barou, C.; Barés, J.; Balme, S.; Garay, H.; Huon, V.; Cornu, D.; Cavaillès, V., et al. Development of new biocompatible 3D printed graphene oxide-based scaffolds. Materials Science and Engineering: C 2020, 110, 110595, doi:https://doi.org/10.1016/j.msec.2019.110595.
6. Belaid, H.; Nagarajan, S.; Barou, C.; Huon, V.; Bares, J.; Balme, S.; Miele, P.; Cornu, D.; Cavaillès, V.; Teyssier, C., et al. Boron Nitride Based Nanobiocomposites: Design by 3D Printing for Bone Tissue Engineering. ACS Applied Bio Materials 2020, 3, 1865-1874, doi:10.1021/acsabm.9b00965.

7. Goh, W.H.; Hashimoto, M. Fabrication of 3D Microfluidic Channels and In-Channel Features Using 3D Printed, Water-Soluble Sacrificial Mold. Macromolecular Materials and Engineering 2018, 303, 1700484, doi:10.1002/mame.201700484.
8. Mohanty, S.; Larsen, L.B.; Trifol, J.; Szabo, P.; Burri, H.V.R.; Canali, C.; Dufva, M.; Emnéus, J.; Wolff, A. Fabrication of scalable and structured tissue engineering scaffolds using water dissolvable sacrificial 3D printed moulds. Materials Science and Engineering: C 2015, 55, 569-578, doi:https://doi.org/10.1016/j.msec.2015.06.002.
9. Lu, R.; Chandrasekaran, S.; Du Frane, W.L.; Landingham, R.L.; Worsley, M.A.; Kuntz, J.D. Complex shaped boron carbides from negative additive manufacturing. Materials & Design 2018, 148, 8-16, doi:https://doi.org/10.1016/j.matdes.2018.03.026.
10. Nejad, H.R.; Sadeqi, A.; Kiaee, G.; Sonkusale, S. Low-cost and cleanroom-free fabrication of microneedles. Microsystems &Amp; Nanoengineering 2018, 4, 17073, doi:10.1038/micronano.2017.73
11. https://www.nature.com/articles/micronano201773#supplementary-information.
12. Yin, J.; Yan, M.; Wang, Y.; Fu, J.; Suo, H. 3D Bioprinting of Low-Concentration Cell-Laden Gelatin Methacrylate (GelMA) Bioinks with a Two-Step Cross-linking Strategy. ACS Applied Materials & Interfaces 2018, 10, 6849-6857, doi:10.1021/acsami.7b16059.
13. Xiao, S.; Zhao, T.; Wang, J.; Wang, C.; Du, J.; Ying, L.; Lin, J.; Zhang, C.; Hu, W.; Wang, L., et al. Gelatin Methacrylate (GelMA)-Based Hydrogels for Cell Transplantation: an Effective Strategy for Tissue Engineering. Stem Cell Reviews and Reports 2019, 15, 664-679, doi:10.1007/s12015-019-09893-4.
14. Mohanty, S.; Sanger, K.; Heiskanen, A.; Trifol, J.; Szabo, P.; Dufva, M.; Emnéus, J.; Wolff, A. Fabrication of scalable tissue engineering scaffolds with dual-pore microarchitecture by combining 3D printing and particle leaching. Materials Science and Engineering: C 2016, 61, 180-189, doi:https://doi.org/10.1016/j.msec.2015.12.032.
15. Li, S.; Liu, Y.-Y.; Liu, L.-J.; Hu, Q.-X. A Versatile Method for Fabricating Tissue Engineering Scaffolds with a Three-Dimensional Channel for Prevasculature Networks. ACS Applied Materials & Interfaces 2016, 8, 25096-25103, doi:10.1021/acsami.6b07725.
16. Jung, J.W.; Lee, H.; Hong, J.M.; Park, J.H.; Shim, J.H.; Choi, T.H.; Cho, D.-W. A new method of fabricating a blend scaffold using an indirect three-dimensional printing technique. Biofabrication 2015, 7, 045003, doi:10.1088/1758-5090/7/4/045003.
17. Bégin-Drolet, A.; Dussault, M.-A.; Fernandez, S.A.; Larose-Dutil, J.; Leask, R.L.; Hoesli, C.A.; Ruel, J. Design of a 3D printer head for additive manufacturing of sugar glass for tissue engineering applications. Additive Manufacturing 2017, 15, 29-39, doi:https://doi.org/10.1016/j.addma.2017.03.006.
18. Gelber, M.K.; Hurst, G.; Comi, T.J.; Bhargava, R. Model-guided design and characterization of a high-precision 3D printing process for carbohydrate glass. Additive Manufacturing 2018, 22, 38-50, doi:https://doi.org/10.1016/j.addma.2018.04.026.
19. Au - Müller, M.; Au - Becher, J.; Au - Schnabelrauch, M.; Au - Zenobi-Wong, M. Printing Thermoresponsive Reverse Molds for the Creation of Patterned Two-component Hydrogels for 3D Cell Culture. JoVE 2013, doi:10.3791/50632, e50632, doi:doi:10.3791/50632.

20. Murphy, C.M.; Haugh, M.G.; O'Brien, F.J. The effect of mean pore size on cell attachment, proliferation and migration in collagen–glycosaminoglycan scaffolds for bone tissue engineering. Biomaterials 2010, 31, 461-466, doi:https://doi.org/10.1016/j.biomaterials.2009.09.063.
21. Muyonga, J.H.; Cole, C.G.B.; Duodu, K.G. Fourier transform infrared (FTIR) spectroscopic study of acid soluble collagen and gelatin from skins and bones of young and adult Nile perch (Lates niloticus). Food Chemistry 2004, 86, 325-332, doi:https://doi.org/10.1016/j.foodchem.2003.09.038.
22. Mansur, H.S.; Sadahira, C.M.; Souza, A.N.; Mansur, A.A.P. FTIR spectroscopy characterization of poly (vinyl alcohol) hydrogel with different hydrolysis degree and chemically crosslinked with glutaraldehyde. Materials Science and Engineering: C 2008, 28, 539-548, doi:https://doi.org/10.1016/j.msec.2007.10.088.
23. Rudra, R.; Kumar, V.; Kundu, P.P. Acid catalysed cross-linking of poly vinyl alcohol (PVA) by glutaraldehyde: effect of crosslink density on the characteristics of PVA membranes used in single chambered microbial fuel cells. RSC Advances 2015, 5, 83436-83447, doi:10.1039/C5RA16068E.
24. Gonzalez-Ortiz, D.; Pochat-Bohatier, C.; Gassara, S.; Cambedouzou, J.; Bechelany, M.; Miele, P. Development of novel h-BNNS/PVA porous membranes via Pickering emulsion templating. Green Chemistry 2018, 20, 4319-4329, doi:10.1039/C8GC01983E.
25. Shen, H.; Hu, X.; Yang, F.; Bei, J.; Wang, S. Combining oxygen plasma treatment with anchorage of cationized gelatin for enhancing cell affinity of poly(lactide-co-glycolide). Biomaterials 2007, 28, 4219-4230, doi:https://doi.org/10.1016/j.biomaterials.2007.06.004.
26. Shu, X.Z.; Liu, Y.; Palumbo, F.; Prestwich, G.D. Disulfide-crosslinked hyaluronan-gelatin hydrogel films: a covalent mimic of the extracellular matrix for in vitro cell growth. Biomaterials 2003, 24, 3825-3834, doi:https://doi.org/10.1016/S0142-9612(03)00267-9.
27. Karageorgiou, V.; Kaplan, D. Porosity of 3D biomaterial scaffolds and osteogenesis. Biomaterials 2005, 26, 5474-5491, doi:https://doi.org/10.1016/j.biomaterials.2005.02.002.
28. Di Luca, A.; Ostrowska, B.; Lorenzo-Moldero, I.; Lepedda, A.; Swieszkowski, W.; Van Blitterswijk, C.; Moroni, L. Gradients in pore size enhance the osteogenic differentiation of human mesenchymal stromal cells in three-dimensional scaffolds. Scientific Reports 2016, 6, 22898, doi:10.1038/srep22898.
29. Qazi, T.H.; Tytgat, L.; Dubruel, P.; Duda, G.N.; Van Vlierberghe, S.; Geissler, S. Extrusion Printed Scaffolds with Varying Pore Size As Modulators of MSC Angiogenic Paracrine Effects. ACS Biomaterials Science & Engineering 2019, 5, 5348-5358, doi:10.1021/acsbiomaterials.9b00843.
30. Jallerat, Q.; Feinberg, A.W. Extracellular Matrix Structure and Composition in the Early Four-Chambered Embryonic Heart. **2020**, *9*, 285, doi: 10.3390/cells9020285
31. Vaitkuviene, A.; Kaseta, V.; Voronovic, J.; Ramanauskaite, G.; Biziuleviciene, G.; Ramanaviciene, A.; Ramanavicius, A. Evaluation of cytotoxicity of polypyrrole nanoparticles synthesized by oxidative polymerization. *Journal of Hazardous Materials* **2013**, *250-251*, 167-174, doi:https://doi.org/10.1016/j.jhazmat.2013.01.038.
32. Ramanaviciene, A.; Kausaite, A.; Tautkus, S.; Ramanavicius, A. Biocompatibility of polypyrrole particles: an in-vivo study in mice. **2007**, *59*, 311-315, doi:https://doi.org/10.1211/jpp.59.2.0017.
33. Vaitkuviene, A.; Ratautaite, V.; Mikoliunaite, L.; Kaseta, V.; Ramanauskaite, G.; Biziuleviciene, G.; Ramanaviciene, A.; Ramanavicius, A. Some biocompatibility aspects of conducting polymer polypyrrole

evaluated with bone marrow-derived stem cells. *Colloids and Surfaces A: Physicochemical and Engineering Aspects* **2014**, *442*, 152-156, doi:https://doi.org/10.1016/j.colsurfa.2013.06.030.

34. Chen, C.; Bai, X.; Ding, Y.; Lee, I.-S. Electrical stimulation as a novel tool for regulating cell behavior in tissue engineering. *Biomaterials Research* **2019**, *23*, 25, doi:10.1186/s40824-019-0176-8.